

Published in final edited form as:

*Acta Biomater.* 2014 December ; 10(12): 4961–4970. doi:10.1016/j.actbio.2014.08.010.

## Mineralized gelatin methacrylate-based matrices induce osteogenic differentiation of human induced pluripotent stem cells

Heemin Kang<sup>a,b</sup>, Yu-Ru V. Shih<sup>a</sup>, Yongsung Hwang<sup>a</sup>, Cai Wen<sup>a,c</sup>, Vikram Rao<sup>a</sup>, Timothy Seo<sup>a,d</sup>, and Shyni Varghese<sup>a,b,d,\*</sup>

Shyni Varghese: svarghese@ucsd.edu

<sup>a</sup>Department of Bioengineering, University of California, San Diego, La Jolla, CA 92093, USA

<sup>b</sup>Materials Science and Engineering Program, University of California, San Diego, La Jolla, CA 92093, USA

<sup>c</sup>School of Chemistry and Chemical Engineering, Southeast University, Nanjing 210018, China

<sup>d</sup>Department of Nanoengineering, University of California, San Diego, La Jolla, CA 92093, USA

### Abstract

Human induced pluripotent stem cells (hiPSCs) are a promising cell source with pluripotency and self-renewal properties. Design of simple and robust biomaterials with an innate ability to induce lineage-specificity of hiPSCs is desirable to realize their applications in regenerative medicine. In this study, we investigated the potential of biomaterials containing calcium phosphate minerals to induce osteogenic differentiation of hiPSCs. hiPSCs cultured using mineralized gelatin methacrylate-based matrices underwent osteogenic differentiation *ex vivo*, both in two-dimensional (2-D) and three-dimensional (3-D) cultures, in growth medium devoid of any osteogenic-inducing chemical components or growth factors. Our findings that osteogenic differentiation of hiPSCs can be achieved through biomaterial-based cues alone present new avenues for personalized regenerative medicine. Such biomaterials that could not only act as structural scaffolds, but could also provide tissue-specific functions such as directing stem cell differentiation commitment, have great potential in bone tissue engineering.

---

© 2014 Elsevier Ltd. All rights reserved.

\*Corresponding author: Associate Professor, Department of Bioengineering, University of California, San Diego, 9500 Gilman Drive, Mail Code 0412, La Jolla, CA 92093-0412, USA, Tel.: +1 858 822 7920, Fax: +1 858 534 5722.

**Conflict of interest:** Authors declare no conflict of interest.

Supplementary data: Supplementary Figures S1-5

Supplementary Table S1

**Publisher's Disclaimer:** This is a PDF file of an unedited manuscript that has been accepted for publication. As a service to our customers we are providing this early version of the manuscript. The manuscript will undergo copyediting, typesetting, and review of the resulting proof before it is published in its final citable form. Please note that during the production process errors may be discovered which could affect the content, and all legal disclaimers that apply to the journal pertain.

## Keywords

Human induced pluripotent stem cells; osteogenic differentiation; calcium phosphate; bone tissue engineering; gelatin methacrylate

---

## 1. Introduction

Human pluripotent stem cells (hPSCs), which include both embryonic stem cells and induced pluripotent stem cells, play an important role in regenerative medicine, developmental biology and pathology, and drug screening owing to their ability to give rise to any cells in the human body and indefinitely self-renew [1, 2]. hiPSCs developed from human autologous somatic cells could circumvent concerns regarding immune properties and ethical issues, making them an ideal cell source for regenerative medicine [3]. Despite the benefits that hiPSCs offer, controlling their differentiation into targeted cell type(s) remains a challenge. Studies over the years have shown that stem cells respond to their microenvironment composed of soluble and matrix-based cues to regulate their fate and commitment [4-6]. Synthetic biomaterials have been extensively used to recapitulate tissue-specific physicochemical cues to direct self-renewal and differentiation of stem cells [7, 8].

Biomaterials containing calcium phosphate minerals have been shown to promote osteogenic differentiation of stem cells [9-14]. These materials have also been shown to support *in vivo* bone tissue formation [11-15]. Previously, we have shown that hydrogels containing acryloyl-6-aminocaproic acid (A6ACA) moieties promote their mineralization when exposed to a medium containing  $\text{Ca}^{2+}$  and  $\text{PO}_4^{3-}$  [16]. The carboxyl groups of A6ACA moieties bind to  $\text{Ca}^{2+}$  ions and promote nucleation and growth of calcium phosphate (CaP) minerals. By employing biomaterialized poly(ethylene glycol)-diacrylate-co-acryloyl-6-aminocaproic acid (PEGDA-co-A6ACA) matrices, we have shown that mineralized matrices can direct osteogenic differentiation of human bone marrow-derived mesenchymal stem cells (hMSCs) and human embryonic stem cells (hESCs) [10, 17]. However, it required the biomaterialized PEGDA-co-A6ACA matrices to be coated with Matrigel to promote initial attachment of the hESCs to the matrix. In this study, we have developed mineralized matrices containing gelatin methacrylate (GelMA) and examined their potential to direct osteogenic differentiation of hiPSCs. Gelatin, derived from natural collagen, possesses cell adhesion motifs that could promote adhesion of hiPSCs to the underlying matrix [18, 19]. Moreover, gelatin-based matrices have been demonstrated to degrade [19-24] and have been studied extensively as a scaffold for tissue engineering [20, 21, 23, 25].

Studies that have reported osteogenic differentiation of hiPSCs often utilized derivation of MSCs or mesoderm-like progenitor cells and their subsequent differentiation into osteoblasts using osteogenic-inducing soluble factors such as  $\beta$ -glycerophosphate, ascorbic acid 2-phosphate, dexamethasone, and/or growth factors like bone morphogenetic protein-2 (BMP-2) [26-32]. A recent study by de Peppo et al. has employed decellularized bone matrix to create bone tissues from hiPSC-derived mesoderm progenitor cells [27]. However, to our knowledge, there are no reports showing osteogenic differentiation of hiPSCs solely through biomaterial-based cues. Here, we demonstrate that biomaterials containing CaP

minerals induce osteogenic differentiation of hiPSCs in growth medium devoid of any osteogenic-inducing small molecules or growth factors.

## 2. Materials and methods

### 2.1. Materials

Synthesis and modification of materials: Poly(ethylene glycol)-diacrylate (PEGDA;  $M_n = 3.4$  kDa) and N-acryloyl 6-aminocaproic acid (A6ACA) were synthesized as previously described [17, 33, 34]. Gelatin-methacrylate (GelMA) was prepared through methacrylation of gelatin (Sigma-Aldrich, catalog number: G1890) [19]. Briefly, 10 g of gelatin along with 100 mL of phosphate buffered saline (PBS) was added into a round-bottom flask purged with argon gas and dissolved under stirring at 60 °C. Around 8 mL of methacrylic anhydride (Polysciences, catalog number: 01517) was added in drop-wise under stirred conditions for 2 hours. The reaction mixture was kept at 60 °C for another 1 hour. 100 mL of pre-warmed PBS at 60 °C was added to the mixture and maintained at 60 °C for 15 minutes. The resulted GelMA was placed in a dialysis tube (Spectrum Laboratories, catalog number: 132676) in deionized (DI) water at 40 °C for 7 days with two daily changes of DI water and filtered through 40  $\mu\text{m}$ -sized pores, lyophilized, and stored at -20 °C prior to use.

### 2.2. Synthesis of gelatin-methacrylate-co-acryloyl 6-aminocaproic acid (GelMA-co-A6ACA) hydrogels

GelMA-co-A6ACA hydrogels were synthesized as follows. 30 w/v% GelMA was dissolved in DI water at 45 °C. 1 M A6ACA was dissolved in 1 M NaOH to deprotonate the carboxyl groups. One part each of 30 w/v% GelMA and 1 M A6ACA were mixed to yield a solution containing 15 w/v% GelMA and 0.5 M (equivalent to 9 w/v%) A6ACA. Around 0.3 w/v% of photoinitiator, 1-[4-(2-Hydroxyethoxy)-phenyl]-2-hydroxy-2-methyl-1-propane-1 (Ciba Specialty Chemicals, Irgacure 2959) in 70% ethanol, was added into the above solution. The solution was then dispensed into a Bio-Rad glass plate separated by a 1-mm spacer and allowed to polymerize at 25 °C under 365 nm UV light for 10 minutes. The resultant hydrogels were incubated in PBS for 24 hours with two changes of PBS. Hydrogels discs of 1  $\text{cm}^2$  (area)  $\times$  1 mm (height) dimensions were used for the cell culture experiments.

### 2.3. Synthesis of gelatin-methacrylate-co-acryloyl 6-aminocaproic acid-co-poly(ethylene glycol)-diacrylate (GelMA-co-A6ACA-co-PEGDA) macroporous hydrogels

GelMA-co-A6ACA-co-PEGDA macroporous hydrogels were synthesized by using polymethylmethacrylate (PMMA) leaching method [35]. First, 8-mm-diameter cylindrical molds packed with PMMA were made from PMMA microspheres having a diameter of 165  $\mu\text{m}$  (Bangs Laboratories, catalog number: BB05N). Each PMMA column was exposed to 60  $\mu\text{l}$  of 20% acetone/80% ethanol mixture for 1 minute to fuse the PMMA beads. The mold was dried at 80 °C for 1 hour and stored at room temperature. Next, 50  $\mu\text{l}$  of a precursor solution containing 10 w/v% GelMA, 9 w/v% A6ACA (treated with NaOH), 10 w/v% PEGDA, and 0.3 w/v% Irgacure 2959 (in 70% ethanol) was dispensed into PMMA-filled molds and photopolymerized using UV light for 10 minutes. The PMMA beads embedded within the GelMA-co-A6ACA-co-PEGDA networks were subsequently dissolved in acetone for 3 days while replenishing fresh acetone three times each day, yielding the macroporous

hydrogels. The resultant macroporous hydrogels were gradually hydrated from pure acetone to acetone/DI water mixture and to pure DI water for a day. The macroporous hydrogels were equilibrated in PBS for 6 hours and punched out to obtain constructs with diameter and height dimensions of 5 mm and 2 mm, respectively.

#### **2.4. Mineralization and sterilization of GelMA-co-A6ACA hydrogels and GelMA-co-A6ACA-co-PEGDA macroporous hydrogels**

GelMA-co-A6ACA hydrogels and GelMA-co-A6ACA-co-PEGDA macroporous hydrogels were subjected to mineralization process as described elsewhere [17]. Briefly, both matrices were soaked in DI water for 6 hours and immersed in modified simulated body fluid (m-SBF; pH=7.4) at 25 °C for 6 hours. The m-SBF solution is composed of 142.0 mM Na<sup>+</sup>, 5.0 mM K<sup>+</sup>, 1.5 mM Mg<sup>2+</sup>, 2.5 mM Ca<sup>2+</sup>, 103.0 mM Cl<sup>-</sup>, 10.0 mM HCO<sub>3</sub><sup>-</sup>, 1.0 mM HPO<sub>4</sub><sup>2-</sup>, and 0.5 mM SO<sub>4</sub><sup>2-</sup> as described elsewhere [36]. The matrices were briefly rinsed with DI water and soaked in 40 mM Ca<sup>2+</sup> and 24 mM HPO<sub>4</sub><sup>2-</sup> solution (pH=5.2) at 25 °C for 45 minutes using VWR Mini Shaker (Catalog number: 12620-938) at 200 rpm. The matrices were then briefly rinsed in DI water, incubated in m-SBF at 37 °C for 2 days with daily change of m-SBF, and equilibrated in PBS for 6 hours.

The mineralized and non-mineralized matrices were sterilized by immersing in 70% ethanol for 6 hours. The ethanol-treated matrices were then washed in sterile PBS by replenishing the PBS four times each day for 4 days to fully remove residual ethanol. Sterile non-mineralized and mineralized GelMA-co-A6ACA hydrogels were employed for 2-D culture. Sterile non-mineralized and mineralized GelMA-co-A6ACA-co-PEGDA macroporous hydrogels were utilized for 3-D culture.

#### **2.5. Scanning electron microscopy (SEM) and energy dispersive spectra (EDS)**

SEM imaging was carried out to investigate the morphology of the mineralized matrices. EDS analysis was performed to determine the composition of the minerals. Samples were briefly rinsed in DI water to remove non-bound ions for 5 minutes, cut into thin slices and subjected to flash-freezing and lyophilization. After Iridium coating for 7 seconds in the sputter (Emitech, K575X), samples were imaged by using SEM (Philips XL30 ESEM) and analyzed for elemental spectra with integrated EDS system. INCA software was used to quantify Ca/P atomic ratio from elemental spectra. The pore diameter of the macroporous matrices was calculated either from SEM or bright field images to estimate the pore structures in the dry and wet state, respectively. Roughly 10 pores were chosen from each of three SEM or bright field images (n=30) and their diameter was determined using ImageJ. The data are presented as mean ± standard errors.

#### **2.6. Calcium and phosphate assays**

Calcium and phosphate assays were conducted to determine the amounts of Ca<sup>2+</sup> and PO<sub>4</sub><sup>3-</sup> in the mineralized matrices and to determine the dissolution of the minerals from the mineralized matrices. The matrices were rinsed in DI water, homogenized and freeze-dried, and their dry weights were measured. To measure the Ca<sup>2+</sup> and PO<sub>4</sub><sup>3-</sup> contents of the mineralized matrices, the dried matrices were subjected to vigorous shaking in 0.5 M HCl at 25 °C for 3 days. To examine the dissolution of CaP minerals from the mineralized matrices

into  $\text{Ca}^{2+}$  and  $\text{PO}_4^{3-}$  in an environment lacking these ions, equilibrium swollen matrices were incubated in 1.5 mL of 50 mM Tris buffer (pH = 7.4), at 37 °C for 7 days and 0.3 mL of incubation medium was collected and replenished with a fresh medium daily. The collected medium was used to measure the dissolution of CaP as a function of the incubation time.

Calcium assay was carried out according to manufacturer's protocol (Calcium reagent set, Pointe Scientific, catalog number: C7503). Briefly, 20  $\mu\text{l}$  of the sample solution was mixed with 1 mL of assay solution containing o-cresolphthalein complexone (CPC). The reaction of calcium with CPC gives rise to a purple color. The absorbance of the resultant product was measured at 570 nm by using a UV/Vis spectrophotometer (Beckman Coulter, DU 730). The absorbance values were compared with those of standard solution at 0, 5, 10, and 15 mg/dl of  $\text{Ca}^{2+}$  in order to determine  $\text{Ca}^{2+}$  content of the sample solution.

Phosphate assay was performed as reported elsewhere [37]. Briefly, the assay solution was prepared by mixing 1 part of 10 mM ammonium molybdate, 2 parts of acetone, and 1 part of 5 N  $\text{H}_2\text{SO}_4$ . 125  $\mu\text{l}$  of the sample solution was mixed with 1 mL of assay solution. To this, 100  $\mu\text{l}$  of 1 M citric acid was added. The absorbance of the resulting solution was measured at 380 nm by using a UV/Vis spectrophotometer. The  $\text{PO}_4^{3-}$  concentration in solution was determined using the standard curve for  $\text{PO}_4^{3-}$ , which was generated for a concentration range of 0-4 mM  $\text{PO}_4^{3-}$ .

## 2.7. Degradation

Non-mineralized and mineralized hydrogels (15% GelMA-co-9% A6ACA in dimensions of 8 mm diameter  $\times$  1 mm height) and macroporous hydrogels (10% GelMA-co-9% A6ACA-co-10% PEGDA in dimensions of 5 mm diameter  $\times$  2 mm height) were examined for their degradation potential prior to cell cultures. All matrices were dried at 37 °C for 24 hours and their dry weights ( $W_{d0}$ ) were measured. The dried matrices were equilibrated in PBS and incubated in 1.5 mL of 0.02 w/v% collagenase type II (Worthington Biochemical, catalog number: LS004177) in PBS at 37 °C [22]. The matrices incubated in 1.5 mL of PBS under identical experimental conditions were used to examine hydrolytic degradation. The incubation solution was replenished with a fresh solution every other day. After 1, 3, 7, and 14 days of incubation, the matrices were collected and briefly rinsed with PBS for 5 minutes to remove any soluble components from degraded matrices. The matrices were dried at 37 °C for 24 hours and their weights ( $W_{dt}$ ) were measured. Weight percentage of the remaining matrix was calculated using the following equation.

$$\text{Weight of remaining matrices (\%)} = \frac{W_{dt}}{W_{d0}} \times 100$$

where  $W_{d0}$  and  $W_{dt}$  represent the weight of the matrix before and after degradation, respectively.

## 2.8. Cell culture

The hiPSC line (IMR90p18-iPS) was procured from WiCell Research Institute, which was generated as described elsewhere [38]. The hiPSCs were maintained on feeder layers of mitotically inactivated mouse embryonic fibroblasts (MEFs) using a medium consisting of knockout DMEM (Life Technologies, catalog number: 10829-018), 10 v/v% knockout serum replacement (Life Technologies, catalog number: 10828028), 10 v/v% human plasmanate (Talecris Biotherapeutics), 1 v/v% non-essential amino acids, 1 v/v% penicillin/streptomycin, 1 v/v% Gluta-MAX, and 55  $\mu\text{M}$  2-mercaptoethanol as previously reported [39]. The medium was changed daily with 30 ng/mL of bFGF (Life Technologies) supplementation.

Cell culture grade glass coverslips (Fisherbrand, catalog number: 1254582) coated with gelatin (Sigma-Aldrich, catalog number: G9391) was used as a control to compare the cellular behaviors on gelatin-based matrices. The gelatin coating of glass coverslips was carried out by incubating the coverslips with 0.1 w/v% gelatin solution at 37 °C for 3 hours. Sterile GelMA-co-A6ACA hydrogels and GelMA-co-A6ACA-co-PEGDA macroporous hydrogels as well as gelatin-coated coverslips were incubated in growth medium composed of DMEM with 10 v/v% FBS (Premium Select; Atlanta Biologicals, catalog number: S11550) at 37 °C for 48 hours prior to cell culture.

For 2-D culture, hiPSCs were seeded onto non-mineralized and mineralized GelMA-co-A6ACA hydrogels and gelatin-coated coverslips at a seeding density of 10,000 cells/cm<sup>2</sup>. Cells were cultured in 1.5 mL of growth medium (high glucose DMEM containing 5 v/v% FBS and 1 v/v% penicillin/streptomycin) at 37 °C and 5% CO<sub>2</sub>. Medium was changed every other day.

For 3-D culture, non-mineralized and mineralized macroporous hydrogels were air-dried at 25 °C for 1 hour. 10  $\mu\text{L}$  of cell suspension containing  $\sim$  300,000 hiPSCs was dispensed into the macroporous hydrogels. The hiPSCs-seeded matrices were incubated at 37°C and 5% CO<sub>2</sub> for 2 hours for cell infiltration. The matrices infiltrated with the cells were cultured in 1.5 mL of growth medium with media change every other day.

## 2.9. Cell Tracker Staining

To visualize cell attachment in 2-D culture, cells were stained with CellTracker (Life Technologies, catalog number: C34552) at 3 days post-plating. Briefly, the cells attached to the matrix were incubated in 20  $\mu\text{M}$  CellTracker reagent in DMEM at 37 °C for 30 minutes and then in growth medium at 37 °C for an additional 30 minutes. The stained cells were imaged using a fluorescence microscope (Carl Zeiss, Axio Observer.A1). The images were used to determine the circularity of the cells using the equation below [10]. 10 cells per image from three different images were used to calculate the area (A) and perimeter (p) of the cells to estimate the circularity (n=30).

$$\text{Circularity} = \frac{4\pi A}{p^2}$$

## 2.10. Reverse Transcription-Polymerase chain reaction (RT-PCR)

PCR analysis was conducted to evaluate time-dependent changes in gene expressions of hiPSCs in 2-D and 3-D cultures. Total RNA was extracted from samples (n= 3 per group per time point) using TRIzol according to manufacturer's protocol. For each sample, 1 µg of RNA was used to synthesize cDNA using iScript cDNA synthesis kit (Bio-rad, catalog number: 170-8891) following manufacturer's protocol. Quantitative RT-PCR measurements were performed using SYBR Select Master Mix (Life technologies, catalog number: 4472908). In addition to Osteogenic PCR array (SA Biosciences, catalog number: PAHS-026), gene expression profile for a number of osteogenic markers (RUNX2, OCN, and SPP1) and pluripotency marker (NANOG) as a function of culture time was carried out. The primer sequences are provided in supplementary Table S1. For PCR array, 84 gene expressions relevant to osteogenic differentiation were profiled and presented as a heat map. The colors of the heat map were scaled according to the relative expression of hiPSCs grown on different matrices (mineralized GelMA-based matrices, non-mineralized GelMA-based matrices, and gelatin-coated coverslips). Red color was assigned to the group with the highest expression while green color was assigned to the group with the lowest expression. The color between red and green was assigned to the group with the intermediate expression level. For RUNX2, OCN, SPP1, and NANOG, the gene expression was normalized to GAPDH, a housekeeping gene. The expression level of each target gene was calculated as  $2^{-Ct}$ . The expression level of hiPSCs grown on various matrices in 2-D and 3-D cultures was normalized to that of undifferentiated, pluripotent hiPSCs and presented as fold expression.

## 2.11. Immunofluorescent staining

The cells cultured on various matrices were fixed with 4% formaldehyde at 25 °C for 7 minutes, washed in PBS, and blocked/permeabilized in a blocking solution of PBS containing 3% BSA and 0.1% Triton-X at 25 °C for 30 minutes. The cells were then incubated with a blocking solution containing primary antibodies against OCT4 (1:200; rabbit polyclonal, Santa Cruz Biotechnology, catalog number: sc-9081), NANOG (1:200; rabbit polyclonal, Santa Cruz Biotechnology, catalog number: sc-33759), or OCN (1:100; mouse monoclonal, Santa Cruz Biotechnology, catalog number: sc-74495) at 4 °C for 16 hours. The cells were washed in PBS and incubated in a blocking solution containing secondary antibody raised against rabbit (1:250; Life Technologies, Alexa Flour 647) or mouse (1:250; Life Technologies, Alexa Flour 568) and phalloidin (1:100; Life Technologies, Alexa Flour 488) at 25 °C for 60 minutes. To counterstain the nuclei, cells were incubated in the Hoechst 33342 solution (2 µg/ml; Life Technologies) at 25 °C for 7 minutes. The images were acquired in a linear mode using the same exposure time for all samples. Using ImageJ software, the background of images was identically subtracted from all images by applying a rolling ball algorithm with rolling ball radius of 750 pixels. To examine autofluorescence of minerals, acellular mineralized matrices were stained at the same time and the images were exposed to the same processing as those with the cells. To evaluate the specificity of osteocalcin antibody, hiPSCs cultured on mineralized matrices for 28 days were stained with secondary antibody without the use of primary antibody and the background of images was subtracted by using the identical method.

### 2.12. Live-dead assay

Live-dead assay was carried out to evaluate the viability and distribution of cells within the macroporous hydrogels after 3 days of cell seeding using Live/Dead Viability/Cytotoxicity kit, (Life technologies, catalog number: L-3224). Briefly, hiPSCs-seeded matrices were washed in PBS and cut into thin slabs. These thin slices were stained using a solution composed of DMEM with 0.05 v/v% green-fluorescent calcein-AM and 0.2 v/v% red-fluorescent ethidium homodimer-1 at 37 °C for 30 minutes. The stained sections were washed with PBS and imaged.

### 2.13. DNA assay

The hiPSCs-seeded macroporous hydrogels were subjected to the DNA assay at 3, 7, and 28 days of culture. The cell-laden matrices were lyophilized and their dry weights were measured. Each lyophilized sample was homogenized in 1 mL of papain solution and incubated at 60 °C for 16 hours. The papain solution was prepared by dissolving 125 µg/mL of papain in a buffer containing 10 mM L-cysteine, 100 mM phosphate, and 10 mM EDTA at pH 6.3. To measure DNA contents of the digested sample, Quant-iT PicoGreen dsDNA assay kit (Life technologies, catalog number: P11496) was used. One part each of digested samples and PicoGreen dsDNA reagent were mixed. Fluorescence of the resulting solution was measured using a microplate reader (Beckman Coulter, DTX 880). Fluorescence values of the samples were compared with those of Lambda DNA standard to quantify the DNA contents of the experimental samples. DNA content of each sample was normalized to the corresponding dry weight.

### 2.14. Immunohistochemical staining

The hiPSCs-laden matrices were fixed with 4% paraformaldehyde at 4 °C for 1 day, demineralized in 10% ethylenediaminetetraacetic acid (EDTA; pH = 7.3) at 4 °C for 3 hours, and equilibrated in PBS for 6 hours. Gradual dehydration of the samples was achieved by immersing them in water/ethanol mixtures and then in pure ethanol for 6 hours. The dehydrated samples were soaked in Citrisolv solution for 1 hour, incubated in a mixture of 95 w/w% paraffin and 5 w/w% poly(ethylene-co-vinyl acetate) (PEVA; Sigma Aldrich, catalog number: 437220) liquid at 70 °C under vacuum for 1 day. The specimens were embedded with paraffin-PEVA mixture through solidification at 25 °C for 1 day. The samples were subsequently sectioned into 10 µm-sized slices using a microtome (Leica, RM2255). The sections were placed into DI water at 40 °C for 5 minutes, then onto charged glass slides, and allowed to dry at 37 °C for 16 hours. The sections on the glass slides were immersed in Citrisolv at 60 °C for 15 minutes with two changes of Citrisolv to remove paraffin-PEVA mixture. The Citrisolv solution was then replaced with pure ethanol. The samples were progressively hydrated by using ethanol/DI water mixtures and followed by DI water.

The sections were incubated in a blocking solution composed of PBS with 3 w/v% BSA and 0.1 v/v% Triton X-100 at 25 °C for 60 minutes and incubated with primary antibody (diluted in blocking solution) against OCN (1:100, mouse monoclonal, Abcam, catalog number: ab13420) at 4 °C for 16 hours. The sections were washed in PBS containing 0.05 v/v% Tween 20 (PBS-Tween 20) three times and treated with 3 v/v% hydrogen peroxide for 7



minutes to deactivate endogenous peroxidases. The sections were then incubated in a blocking buffer containing horseradish peroxidase (HRP)-conjugated secondary antibody against mouse (1:100, Santa Cruz Biotechnology, catalog number: sc-2005) at 25 °C for 60 minutes. The sections were washed in PBS-Tween20 three times and exposed to a developing solution containing 3-3' diaminobenzidine (DAB) substrate (Vector Laboratories, catalog number: SK-4100) for 7 minutes, washed in PBS-Tween 20 three times, and subsequently imaged using a microscope in color mode.

### 2.15. Statistical analysis

Statistical analyses were performed using GraphPad Prism (version 5.00) software. Statistical significances were assigned for p-values less than 0.05. The asterisks were assigned to further demonstrate different degrees of statistical significances. Three different statistical methods were used to compare groups in various combinations. Two-tailed Student's t-test was employed to compare two groups at the same time point. One-way analysis of variance (ANOVA) with Tukey-Kramer post-hoc test was used to compare multiple groups at the same time point. Two-way ANOVA with Bonferroni post-hoc test was utilized to compare multiple groups at various time points.

## 3. Results

### 3.1. Synthesis, characterization, and degradation of mineralized matrices

Hydrogels and macroporous hydrogels were used for 2-D and 3-D cultures, respectively. The hydrogel and macroporous matrices were mineralized to incorporate calcium phosphate moieties. Both mineralized hydrogels and macroporous hydrogels were found to be opaque in contrast to the transparent non-mineralized counterparts (Supplementary Figs. S1a, S2a). Scanning electron microscopy (SEM) images of the mineralized hydrogels and macroporous hydrogels showed matrix-bound minerals having a plate-like morphology; no such features were present in the corresponding non-mineralized controls (Fig. 1a,e). Elemental dispersive spectra (EDS) revealed the presence of calcium and phosphorus elements in mineralized matrices with a Ca/P ratio of 0.99 and 1.42 for the mineralized hydrogels and macroporous hydrogels, respectively. As expected, no calcium or phosphorus elements were detected in their non-mineralized counterparts. As evident from  $\text{Ca}^{2+}$  and  $\text{PO}_4^{3-}$  measurements, the mineralized hydrogels contained  $32.2 \pm 1.5$  and  $50.3 \pm 4.8$  mg of  $\text{Ca}^{2+}$  and  $\text{PO}_4^{3-}$  per gram of dry weight, respectively (Supplementary Fig. S1b-c). Similarly, the mineralized macroporous hydrogels had  $68.4 \pm 4.2$  and  $112.3 \pm 4.7$  mg of  $\text{Ca}^{2+}$  and  $\text{PO}_4^{3-}$  per gram of dry weight, respectively (Supplementary Fig. S2c-d). Concurrent with previous findings, the CaP moieties of the mineralized matrices (mineralized hydrogels and macroporous hydrogels) dissociated into  $\text{Ca}^{2+}$  and  $\text{PO}_4^{3-}$  ions in a medium lacking these components (Fig. 1b-c,f-g) [17]. Both mineralized hydrogels and macroporous hydrogels exhibited a rapid release of  $\text{Ca}^{2+}$  and  $\text{PO}_4^{3-}$  ions within 1 day followed by a slow release of  $\text{Ca}^{2+}$  and no significant release of  $\text{PO}_4^{3-}$  for 7 days.

Both non-mineralized and mineralized macroporous hydrogels exhibited interconnected pores as evident from the SEM images (Fig. 1e). Furthermore, the pore diameter of the macroporous hydrogels in their dried state, estimated from the SEM images, was  $50.2 \pm 3.0$

$\mu\text{m}$ . The pore diameter of the non-mineralized and mineralized macroporous hydrogels in their swollen state, estimated from the bright field images, was  $117.7 \pm 5.7$  and  $115.2 \pm 6.4$   $\mu\text{m}$ , respectively (Supplementary Fig. S2b).

The ability to degrade in presence of collagenase is a characteristic of gelatin-based scaffolds. To evaluate the effect of mineralization on degradation of GelMA-based matrices, the mineralized and non-mineralized hydrogels and macroporous hydrogels were incubated in PBS or PBS containing collagenase type II. Enzymatic degradation of non-mineralized and mineralized GelMA-based hydrogels with collagenase type II resulted in  $\sim 29\%$  and  $25\%$  of mass loss by 14 days, respectively, while their incubation in PBS exhibited less than  $10\%$  of mass loss during the same time period (Fig. 1d). A similar degradation pattern was observed for macroporous hydrogels (Fig. 1h). Enzyme-mediated degradation of non-mineralized and mineralized GelMA-based macroporous hydrogels yielded  $\sim 30\%$  and  $25\%$  of mass loss after 14 days of incubation in collagenase type II, respectively. The hydrolytic degradation of such macroporous matrices was found to be negligible during 14 days of incubation in PBS.

### 3.2. Attachment, proliferation, and osteogenic differentiation of hiPSCs on mineralized matrices in 2-D culture

The pluripotency of hiPSCs prior to their culture on various matrices was confirmed by immunofluorescent staining for OCT4 and NANOG, well-established pluripotent markers (Supplementary Fig. S3) [39]. The pluripotent hiPSCs were seeded onto mineralized and non-mineralized GelMA-co-A6ACA hydrogel matrices as well as gelatin-coated coverslips. The adhesion and growth of hiPSCs on mineralized GelMA-co-A6ACA hydrogels were examined and compared against those on non-mineralized hydrogels and gelatin-coated coverslips as a function of culture time (Fig. 2a-b). All matrices supported the attachment of hiPSCs within 3 days of culture with no significant differences in cell adhesion (Fig. 2a). The cell shape measured in terms of circularity suggests that cells on all matrices spread and acquired similar shape within 3 days of plating (Fig. 2b). By 10 days of culture, hiPSCs on all the matrices grew to reach confluence (Fig. 2a). Having verified that all matrices under investigation support the attachment and proliferation of hiPSCs in similar extents, we next evaluated the osteogenic differentiation of hiPSCs on various matrices. After 28 days of culture, PCR array revealed that the cells on mineralized matrices exhibited an upregulation of various genes relevant to cells undergoing osteogenesis compared to those on non-mineralized matrices and gelatin-coated coverslips (Fig. 3a). The gene profile was further verified through time course analyses of different osteogenic gene markers and it was found that the cells on mineralized matrices showed higher expression of RUNX2, OCN, and SPP1 compared to those on non-mineralized and coverslip groups throughout 28 days of culture (Fig. 3b-d). Immunofluorescent staining for OCN in hiPSCs on mineralized hydrogels revealed positive staining after 28 days of culture, which was not detected on non-mineralized hydrogels or coverslips (Fig. 3e and Supplementary Fig. S4). Moreover, OCN staining intensity was found to gradually increase for hiPSCs on mineralized hydrogels with culture time (Supplementary Fig. S5a). The corresponding Hoechst and F-actin staining of the cells on various matrices as a function of culture time are also shown (Supplementary Fig. S5a-b). The hiPSCs cultured on all matrices exhibited the downregulation of NANOG

expression compared to pluripotent hiPSCs prior to their culture on various matrices (Supplementary Fig. S5c).

### 3.3. Osteogenic differentiation of hiPSCs on mineralized macroporous matrices in 3-D culture

We next determined the potential of 3-D mineralized matrices in directing osteogenic commitment of hiPSCs by using mineralized GelMA-co-A6ACA-co-PEGDA macroporous hydrogels. The PEGDA molecules were incorporated to optimize pore interconnectivity and robustness of the macroporous matrices. The mineralized matrix-induced osteogenic differentiation was compared against that of corresponding non-mineralized macroporous hydrogels. Live-dead staining of hiPSC-laden matrices after 3 days of cell seeding demonstrated homogeneous distribution for a majority of live cells within the non-mineralized and mineralized matrices (Fig. 4a). While both matrices supported cell survival, there were distinct differences in cell shape and cell-matrix interactions. Most cells within the non-mineralized matrices were aggregated to form small clusters while those within the mineralized matrices were found to spread on the pore walls of the matrices. Despite the differences in cell shape and adhesion between two matrices, DNA assay showed similar DNA contents of hiPSCs cultured in both non-mineralized and mineralized matrices at all experimental time points, suggesting that similar cell numbers were maintained between the mineralized and non-mineralized matrices (Fig. 4b). Time-resolved gene expression of osteogenic markers for RUNX2, OCN, and SPP1 revealed significant upregulation of these markers in cells on mineralized matrices compared to those on non-mineralized matrices, akin to 2-D culture (Fig. 4c-e). Immunohistochemical staining for OCN further corroborated the gene expression pattern as prevalent staining for OCN was observed in mineralized matrices, which remained absent in non-mineralized counterparts (Fig. 4g). Furthermore, pervasiveness of OCN stains in mineralized matrices progressively increased with culture time. Although only the hiPSCs on mineralized macroporous matrices were found to differentiate into osteoblasts, cells cultured in all macroporous matrices showed a significant downregulation of NANOG expression, similar to 2-D culture (Fig. 4f).

## 4. Discussion

The potential of biomaterials in directing stem cell differentiation continues to be revealed, leading to new possibilities in regenerative medicine. Human pluripotent stem cells, such as hiPSCs that offer a unique cell source, in conjunction with biomaterials, could be powerful in treating compromised tissues and organs. Studies over the years have designed biomaterials with defined physicochemical cues to direct differentiation of stem cells into targeted phenotypes. Previously, we have shown that biomaterials containing CaP moieties promote osteogenic commitment of stem cells both *in vitro* and *in vivo* [10, 11, 17]. Here, by employing a mineralized GelMA-based matrix, we ask whether matrix-based cues alone can direct differentiation of pluripotent hiPSCs into osteoblasts.

Human iPSCs grown on GelMA-based matrices in 2-D culture demonstrated similar levels of attachment, spreading, and proliferation in growth medium. Though all the matrices supported the adhesion and growth of hiPSCs to similar extents, only the cells on mineralized matrices were found to undergo osteogenic differentiation. hiPSCs on

mineralized matrices after 28 days of culture in a 2-D setting demonstrated intense staining for OCN, an osteoblast marker, coincident with F-actin staining in a majority of the cells. This finding suggests efficient osteogenic differentiation of hiPSCs in a mineralized environment. Previous studies demonstrated that biomaterial-assisted osteogenic differentiation of stem cells in 2-D culture was accompanied by changes in cell shape [40]. However, our findings that cells only on the mineralized matrices underwent osteogenic differentiation despite cells on all matrices having similar shape suggest that the observed osteogenic differentiation of hiPSCs on mineralized matrices is not attributed to the cell shape. This finding further implies that the osteogenic differentiation of hiPSCs observed on mineralized matrices is mainly attributed to the mineral environment-mediated differentiation cues. Similar results were also observed with 3-D culture, albeit within disparate spatial geometry in the culture. The findings that hiPSCs undergo osteogenic differentiation on CaP-rich GelMA-based matrices in 2-D and 3-D culture conditions are consistent with our previous findings that CaP-rich PEGDA-based matrices promote osteogenic differentiation of hMSCs and hESCs [10, 11, 17]. Together, these studies suggest that mineralized matrices containing CaP moieties offer a robust environment to support osteogenic commitment of stem cells despite the differences in the organic moieties of the scaffold.

In contrast to 2-D culture, cells in 3-D macroporous hydrogels showed significant differences in their attachment; cells on mineralized matrices exhibited more spread morphology whereas those on non-mineralized matrices showed aggregation. These results suggest enhanced cell-matrix interactions on mineralized macroporous matrices compared to their non-mineralized counterparts. The reason behind the observed difference between 2-D and 3-D cultures is not apparent. The hiPSCs cultured in all matrices showed significant downregulation of NANOG expression, indicating that all the matrices and culture conditions used in this study are not conducive for the maintenance of pluripotency. This is in agreement with previous studies that showed the importance of a delicate balance in physicochemical cues of the matrix on the maintenance of pluripotency for hiPSCs [39].

Although a number of studies have shown that materials containing CaP moieties promote osteogenic differentiation of progenitor cells and contribute to *in vivo* bone tissue repair, recent studies suggest that the osteoinductive function of such matrices is dependent upon their ability to regulate extracellular  $\text{Ca}^{2+}$  and  $\text{PO}_4^{3-}$  [9, 12]. This could partially explain the different extents of osteogenic outcomes observed among CaP-based matrices with different levels of crystallinity and composition, owing to disparate dissociation kinetics of CaP minerals into  $\text{Ca}^{2+}$  and  $\text{PO}_4^{3-}$ . Osathanon et al. previously reported that CaP-rich biomineralized matrices exhibiting faster dissolution rates have higher osteostimulatory effect on osteoblast-like cells when compared with hydroxyapatite-incorporated matrices [41]. Results from our dissolution studies suggest that the CaP minerals of the mineralized matrices readily dissociate into  $\text{Ca}^{2+}$  and  $\text{PO}_4^{3-}$  ions in a permissive environment. The extracellular  $\text{Ca}^{2+}$  and  $\text{PO}_4^{3-}$  ions have been shown to promote osteogenic commitment of stem cells through various signaling pathways. Studies by Wen et al. have shown that extracellular  $\text{Ca}^{2+}$  promotes osteogenic differentiation of MSCs through L-type calcium channels [42]. Recently, we have shown that mineralized matrices containing CaP moieties

could direct osteogenic differentiation of stem cells through adenosine signaling [43]. In addition, the dissolution and re-precipitation of CaP minerals can adsorb and release osteoinductive growth factors [44-46]. All of these factors could be contributing to the observed CaP-bearing matrices-induced osteogenic commitment of hiPSCs.

## 5. Conclusion

In summary, the results described in this study show that mineralized GelMA-based matrices containing CaP mineral direct osteogenic differentiation commitment of hiPSCs in growth medium lacking osteoinductive soluble factors. To our knowledge, this is the first demonstration of osteogenic differentiation of hiPSCs by inherent material-based cues. Future work includes the transplantation of hiPSCs with GelMA-based matrices *in vivo* to study the effect of minerals and degradation on the osteogenic differentiation of hiPSCs and bone tissue formation.

## Supplementary Material

Refer to Web version on PubMed Central for supplementary material.

## Acknowledgments

Authors gratefully acknowledge the financial support from National Institutes of Health and California Institute of Regenerative Medicine (NIH, Grant 1 R01 AR063184-01A1; CIRM, RN2-00945 and RT2-01889).

## References

1. Amabile G, Meissner A. Induced pluripotent stem cells: current progress and potential for regenerative medicine. *Trends in molecular medicine*. 2009; 15:59–68. [PubMed: 19162546]
2. Wobus AM, Boheler KR. Embryonic stem cells: prospects for developmental biology and cell therapy. *Physiological reviews*. 2005; 85:635–78. [PubMed: 15788707]
3. Takahashi K, Tanabe K, Ohnuki M, Narita M, Ichisaka T, Tomoda K, et al. Induction of pluripotent stem cells from adult human fibroblasts by defined factors. *cell*. 2007; 131:861–72. [PubMed: 18035408]
4. Teng S, Liu C, Krettek C, Jagodzinski M. The Application of Induced Pluripotent Stem Cells for Bone Regeneration: Current Progress and Prospects. *Tissue Engineering Part B: Reviews*. 2013
5. Illich DJ, Demir N, Stojkovi M, Scheer M, Rothamel D, Neugebauer J, et al. Concise review: induced pluripotent stem cells and lineage reprogramming: prospects for bone regeneration. *Stem Cells*. 2011; 29:555–63. [PubMed: 21308867]
6. Discher DE, Mooney DJ, Zandstra PW. Growth factors, matrices, and forces combine and control stem cells. *Science*. 2009; 324:1673–7. [PubMed: 19556500]
7. Hwang Y, Phadke A, Varghese S. Engineered microenvironments for self-renewal and musculoskeletal differentiation of stem cells. *Regenerative Medicine*. 2011; 6:505–24. [PubMed: 21749208]
8. Saha K, Pollock JF, Schaffer DV, Healy KE. Designing synthetic materials to control stem cell phenotype. *Current opinion in chemical biology*. 2007; 11:381–7. [PubMed: 17669680]
9. LeGeros RZ. Calcium phosphate-based osteoinductive materials. *Chemical reviews*. 2008; 108:4742–53. [PubMed: 19006399]
10. Phadke A, Shih YR, Varghese S. Mineralized synthetic matrices as an instructive microenvironment for osteogenic differentiation of human mesenchymal stem cells. *Macromolecular bioscience*. 2012; 12:1022–32. [PubMed: 22760917]

11. Phadke A, Hwang Y, Hee Kim S, Hyun Kim S, Yamaguchi T, Masuda K, et al. Effect of scaffold microarchitecture on osteogenic differentiation of human mesenchymal stem cells. *European cells & materials*. 2013; 25:114–29. [PubMed: 23329467]
12. Yuan H, Fernandes H, Habibovic P, de Boer J, Barradas AM, de Ruiter A, et al. Osteoinductive ceramics as a synthetic alternative to autologous bone grafting. *Proceedings of the National Academy of Sciences*. 2010; 107:13614–9.
13. Vaquette C, Ivanovski S, Hamlet SM, Hutmacher DW. Effect of culture conditions and calcium phosphate coating on ectopic bone formation. *Biomaterials*. 2013; 34:5538–51. [PubMed: 23623428]
14. Seyedjafari E, Soleimani M, Ghaemi N, Shabani I. Nanohydroxyapatite-coated electrospun poly (l-lactide) nanofibers enhance osteogenic differentiation of stem cells and induce ectopic bone formation. *Biomacromolecules*. 2010; 11:3118–25. [PubMed: 20925348]
15. Song G, Habibovic P, Bao C, Hu J, van Blitterswijk CA, Yuan H, et al. The homing of bone marrow MSCs to non-osseous sites for ectopic bone formation induced by osteoinductive calcium phosphate. *Biomaterials*. 2013; 34:2167–76. [PubMed: 23298780]
16. Phadke A, Zhang C, Hwang Y, Vecchio K, Varghese S. Templated mineralization of synthetic hydrogels for bone-like composite materials: Role of matrix hydrophobicity. *Biomacromolecules*. 2010; 11:2060–8. [PubMed: 20690714]
17. Kang H, Wen C, Hwang Y, Shih YRV, Kar M, Seo SW, et al. Biomineralized matrix-assisted osteogenic differentiation of human embryonic stem cells. *Journal of Materials Chemistry B*. 2014
18. Heino J. The collagen family members as cell adhesion proteins. *Bioessays*. 2007; 29:1001–10. [PubMed: 17876790]
19. Hutson CB, Nichol JW, Aubin H, Bae H, Yamanlar S, Al-Haque S, et al. Synthesis and characterization of tunable poly (ethylene glycol): gelatin methacrylate composite hydrogels. *Tissue Engineering Part A*. 2011; 17:1713–23. [PubMed: 21306293]
20. Chen YC, Lin RZ, Qi H, Yang Y, Bae H, Melero-Martin JM, et al. Functional human vascular network generated in photocrosslinkable gelatin methacrylate hydrogels. *Advanced functional materials*. 2012; 22:2027–39. [PubMed: 22907987]
21. Talwar R, Di Silvio L, Hughes FJ, King GN. Effects of carrier release kinetics on bone morphogenetic protein-2-induced periodontal regeneration in vivo. *Journal of clinical periodontology*. 2001; 28:340–7. [PubMed: 11314890]
22. Park KM, Lee Y, Son JY, Oh DH, Lee JS, Park KD. Synthesis and characterizations of in situ cross-linkable gelatin and 4-arm-PPO-PEO hybrid hydrogels via enzymatic reaction for tissue regenerative medicine. *Biomacromolecules*. 2012; 13:604–11. [PubMed: 22263670]
23. Benton JA, DeForest CA, Vivekanandan V, Anseth KS. Photocrosslinking of gelatin macromers to synthesize porous hydrogels that promote valvular interstitial cell function. *Tissue Engineering Part A*. 2009; 15:3221–30. [PubMed: 19374488]
24. Yaylao lu M, Korkusuz P, Örs Ü, Korkusuz F, Hasirci V. Development of a calcium phosphate-gelatin composite as a bone substitute and its use in drug release. *Biomaterials*. 1999; 20:711–9. [PubMed: 10353654]
25. Nichol JW, Koshy ST, Bae H, Hwang CM, Yamanlar S, Khademhosseini A. Cell-laden microengineered gelatin methacrylate hydrogels. *Biomaterials*. 2010; 31:5536–44. [PubMed: 20417964]
26. Zou L, Luo Y, Chen M, Wang G, Ding M, Petersen CC, et al. A simple method for deriving functional MSCs and applied for osteogenesis in 3D scaffolds. *Scientific reports*. 2013:3.
27. de Peppo GM, Marcos-Campos I, Kahler DJ, Alsalman D, Shang L, Vunjak-Novakovic G, et al. Engineering bone tissue substitutes from human induced pluripotent stem cells. *Proceedings of the National Academy of Sciences*. 2013; 110:8680–5.
28. Ardehshiryajimi A, Dinarvand P, Seyedjafari E, Langroudi L, Adegani FJ, Soleimani M. Enhanced reconstruction of rat calvarial defects achieved by plasma-treated electrospun scaffolds and induced pluripotent stem cells. *Cell and tissue research*. 2013; 354:849–60. [PubMed: 23955642]
29. Ardehshiryajimi A, Hosseinkhani S, Parivar K, Yaghmaie P, Soleimani M. Nanofiber-based polyethersulfone scaffold and efficient differentiation of human induced pluripotent stem cells into osteoblastic lineage. *Molecular biology reports*. 2013:1–8. [PubMed: 23135731]

30. Kang R, Luo Y, Zou L, Xie L, Lysdahl H, Jiang X, et al. Osteogenesis of human induced pluripotent stem cells derived mesenchymal stem cells on hydroxyapatite contained nanofibers. *RSC Advances*. 2014; 4:5734–9.
31. Liu J, Chen W, Zhao Z, Xu HH. Reprogramming of mesenchymal stem cells derived from iPSCs seeded on biofunctionalized calcium phosphate scaffold for bone engineering. *Biomaterials*. 2013; 34:7862–72. [PubMed: 23891395]
32. Levi B, Hyun JS, Montoro DT, Lo DD, Chan CK, Hu S, et al. In vivo directed differentiation of pluripotent stem cells for skeletal regeneration. *Proceedings of the National Academy of Sciences*. 2012; 109:20379–84.
33. Hwang Y, Zhang C, Varghese S. Poly (ethylene glycol) cryogels as potential cell scaffolds: effect of polymerization conditions on cryogel microstructure and properties. *Journal of Materials Chemistry*. 2010; 20:345–51.
34. Ayala R, Zhang C, Yang D, Hwang Y, Aung A, Shroff SS, et al. Engineering the cell-material interface for controlling stem cell adhesion, migration, and differentiation. *Biomaterials*. 2011; 32:3700–11. [PubMed: 21396708]
35. Bryant SJ, Cuy JL, Hauch KD, Ratner BD. Photo-patterning of porous hydrogels for tissue engineering. *Biomaterials*. 2007; 28:2978–86. [PubMed: 17397918]
36. Oyane A, Kim HM, Furuya T, Kokubo T, Miyazaki T, Nakamura T. Preparation and assessment of revised simulated body fluids. *Journal of Biomedical Materials Research Part A*. 2003; 65:188–95. [PubMed: 12734811]
37. Heinonen JK, Lahti RJ. A New and Convenient Colorimetric Determination of Inorganic Ortho-Phosphate and Its Application to the Assay of Inorganic Pyrophosphatase. *Analytical Biochemistry*. 1981; 113:313–7. [PubMed: 6116463]
38. Yu J, Vodyanik MA, Smuga-Otto K, Antosiewicz-Bourget J, Frane JL, Tian S, et al. Induced pluripotent stem cell lines derived from human somatic cells. *Science*. 2007; 318:1917–20. [PubMed: 18029452]
39. Chang CW, Hwang Y, Brafman D, Hagan T, Phung C, Varghese S. Engineering cell-material interfaces for long-term expansion of human pluripotent stem cells. *Biomaterials*. 2013; 34:912–21. [PubMed: 23131532]
40. McBeath R, Pirone DM, Nelson CM, Bhadriraju K, Chen CS. Cell shape, cytoskeletal tension, and RhoA regulate stem cell lineage commitment. *Developmental cell*. 2004; 6:483–95. [PubMed: 15068789]
41. Osathanon T, Linnes ML, Rajachar RM, Ratner BD, Somerman MJ, Giachelli CM. Microporous nanofibrous fibrin-based scaffolds for bone tissue engineering. *Biomaterials*. 2008; 29:4091–9. [PubMed: 18640716]
42. Wen L, Wang Y, Wang H, Kong L, Zhang L, Chen X, et al. L-type calcium channels play a crucial role in the proliferation and osteogenic differentiation of bone marrow mesenchymal stem cells. *Biochemical and Biophysical Research Communications*. 2012; 424:439–45. [PubMed: 22771798]
43. Shih YRV, Hwang Y, Phadke A, Kang H, Hwang NS, Caro EJ, et al. Calcium phosphate-bearing matrices induce osteogenic differentiation of stem cells through adenosine signaling. *Proceedings of the National Academy of Sciences*. 2014; 111:990–5.
44. Suarez-Gonzalez D, Barnhart K, Migneco F, Flanagan C, Hollister SJ, Murphy WL. Controllable mineral coatings on PCL scaffolds as carriers for growth factor release. *Biomaterials*. 2012; 33:713–21. [PubMed: 22014948]
45. Suárez-González D, Lee JS, Lan Levensgood SK, Vanderby R Jr, Murphy WL. Mineral coatings modulate  $\beta$ -TCP stability and enable growth factor binding and release. *Acta biomaterialia*. 2012; 8:1117–24. [PubMed: 22154864]
46. Autefage H, Briand-Mesange F, Cazalbou S, Drouet C, Fourmy D, Goncalves S, et al. Adsorption and release of BMP-2 on nanocrystalline apatite-coated and uncoated hydroxyapatite/beta-tricalcium phosphate porous ceramics. *Journal of biomedical materials research Part B, Applied biomaterials*. 2009; 91:706–15.

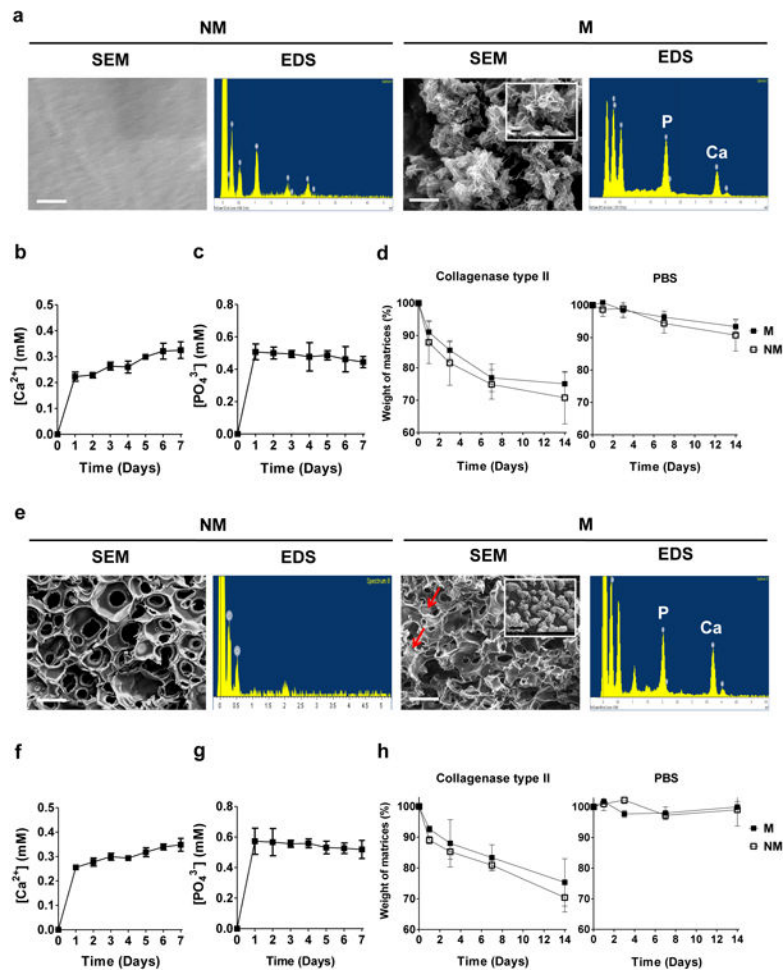


**Figure 1. Development and characterization of GelMA-based matrices**

(a) SEM images and corresponding EDS for non-mineralized (NM) and mineralized (M) gelatin-methacrylate-co-acryloyl 6-aminocaproic acid (GelMA-co-A6ACA) hydrogels. Scale bar: 1  $\mu\text{m}$ . Inset shows high magnification image. Scale bar: 200 nm. Dissolution of (b)  $\text{Ca}^{2+}$  and (c)  $\text{PO}_4^{3-}$  from mineralized GelMA-co-A6ACA hydrogels incubated in Tris-HCl buffer at 37  $^{\circ}\text{C}$  as a function of time. (d) In vitro degradation of non-mineralized and mineralized GelMA-co-A6ACA hydrogels in 0.02 w/v% collagenase type II solution or PBS at 37  $^{\circ}\text{C}$  as a function of time. (e) SEM images and corresponding EDS for non-mineralized and mineralized gelatin-methacrylate-co-acryloyl 6-aminocaproic acid-co-poly(ethylene glycol)-diacrylate (GelMA-co-A6ACA-co-PEGDA) macroporous hydrogels. Red arrows indicate mineral structures. Scale bar: 100  $\mu\text{m}$ . Inset shows high magnification image. Scale bar: 1  $\mu\text{m}$ . Release of (f)  $\text{Ca}^{2+}$  and (g)  $\text{PO}_4^{3-}$  from mineralized GelMA-co-A6ACA-co-PEGDA macroporous hydrogels in Tris-HCl buffer at 37  $^{\circ}\text{C}$  as a function of time. (h) In vitro degradation of non-mineralized and mineralized GelMA-co-A6ACA-co-PEGDA macroporous hydrogels in 0.02 w/v% collagenase type II solution or PBS at 37  $^{\circ}\text{C}$  as a function of time. Data are presented as mean  $\pm$  standard errors ( $n=3$ ).



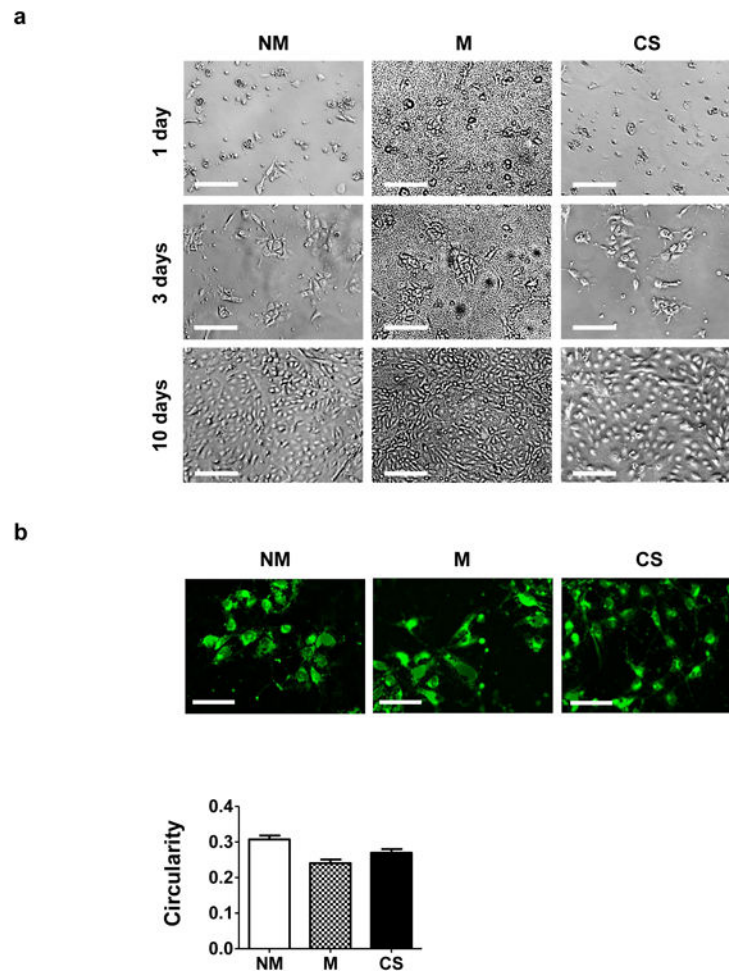


**Figure 2. Attachment and proliferation of hiPSCs on different matrices**

(a) Bright field images for hiPSCs after 1, 3, and 10 days of culture on non-mineralized (NM) and mineralized (M) hydrogels and gelatin-coated coverslips (CS). Scale bar: 200  $\mu\text{m}$ .

(b) Images of hiPSCs labeled using CellTracker after 3 days of culture on non-mineralized and mineralized hydrogels and coverslips. Scale bar: 100  $\mu\text{m}$ . The bar graph shows the quantitative representation of the circularity; the circularity indices were determined from the stained images. Data are shown as mean  $\pm$  standard errors (n=30).

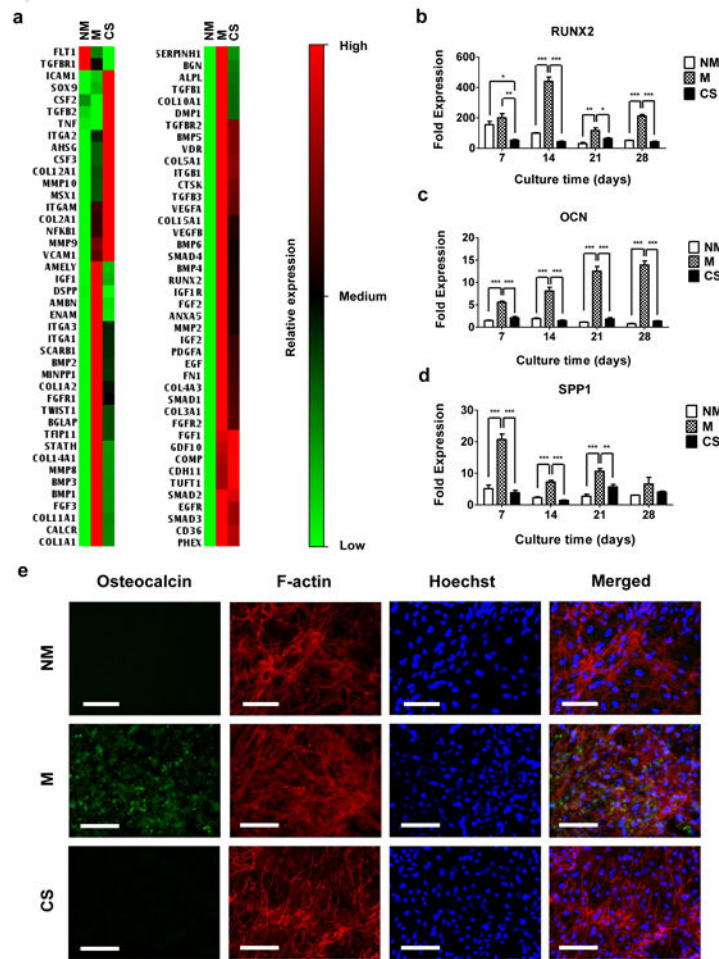


**Figure 3. Osteogenic differentiation of hiPSCs on CaP-rich mineralized hydrogels in 2-D culture** (a) Gene expression array analyses of hiPSCs cultured for 28 days on non-mineralized (NM) and mineralized (M) hydrogels and coverslips (CS). Relative expressions: red (high), black (medium), and green (low). Gene expressions of (b) RUNX2, (c) OCN, and (d) SPP1 for hiPSCs cultured on non-mineralized and mineralized hydrogels and coverslips as a function of culture time. Data are presented as fold expression of target genes after normalization to undifferentiated, pluripotent hiPSCs. (e) Immunofluorescent staining for OCN (green) and F-actin (red) of hiPSCs cultured on non-mineralized and mineralized hydrogels and coverslips for 28 days. Nuclei are stained blue with Hoechst. Scale bars represent 100  $\mu$ m. Data are displayed as mean  $\pm$  standard errors (n=3). (b-d) Comparison of multiple groups at the same time point was made by one-way ANOVA with Tukey-Kramer post-hoc test. Asterisks indicate statistical significances corresponding to p-values (\*:  $p < 0.05$ ; \*\*:  $p < 0.01$ ; \*\*\*:  $p < 0.001$ ).

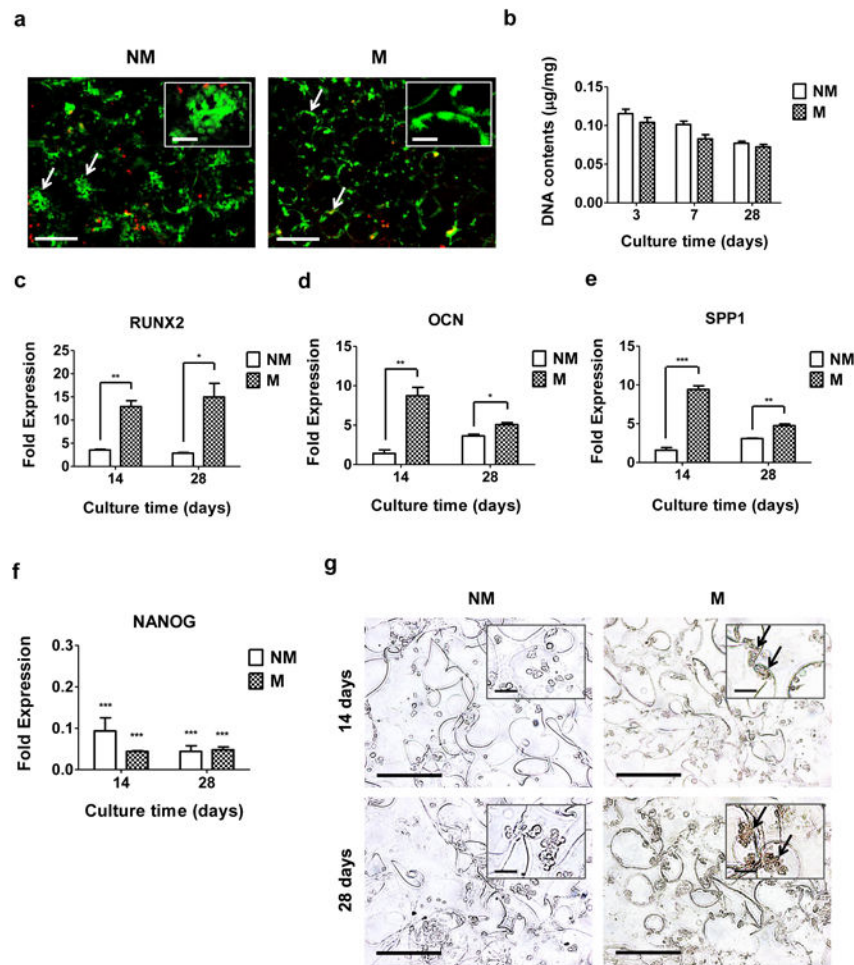


**Figure 4. Osteogenic differentiation of hiPSCs on CaP-rich mineralized macroporous hydrogels in 3-D culture**

(a) Live-dead staining of hiPSC-laden non-mineralized (NM) and mineralized (M) macroporous hydrogels after 3 days of culture. Arrows and inset indicate aggregated and spread hiPSCs within the non-mineralized and mineralized matrices, respectively. Scale bars represent 200  $\mu\text{m}$  and scale bars in the inset indicate 50  $\mu\text{m}$ . (b) DNA contents of hiPSCs cultured using non-mineralized and mineralized matrices as a function of culture time. Data are presented as DNA contents after normalization to dry weight of matrices. Gene expression of (c) RUNX2, (d) OCN, (e) SPP1, and (f) NANOG of hiPSCs on non-mineralized and mineralized matrices as a function of culture time. Data are presented as fold expression of target genes after normalization to undifferentiated, pluripotent hiPSCs. (g) Immunohistochemical staining for OCN of hiPSCs on non-mineralized and mineralized matrices as a function of culture time. Scale bars represent 100  $\mu\text{m}$ . Inset shows high magnification images. Arrows indicate positive stains. Scale bars in the inset represent 20  $\mu\text{m}$ . Data are displayed as mean  $\pm$  standard errors ( $n=3$ ). (c-e) Two groups at the same time point were compared by two-tailed Student's t-test. (f) All the groups were compared to undifferentiated, pluripotent hiPSCs prior to their culture on all matrices by two-way

ANOVA with Bonferroni post-hoc test. Asterisks represent statistical significances according to p-values. (\*:  $p < 0.05$ ; \*\*:  $p < 0.01$ ; \*\*\*:  $p < 0.001$ ).